# Analysis of failure behavior of shear connection in push-out specimen by three-dimensional stress analysis

[*]Hyun-Seop Shin[1]

[1]*Structural Engineering Research Division, Korea Institute of Civil Engineering and Building Technology,
283 Goyangdae-Ro, Ilsanseo-Gu, Goyang-Si, Gyeonggi-Do, 10223, South Korea*
*Corresponding author: *Hyun-Seop Shin*

**ABSTRACT:-** This study analyzes the failure mechanism of shear connection by three-dimensional finite element analysis (FEA) of push-out specimens that was practically unaffordable experimentally or by two-dimensional FEA. For the analysis of the failure behavior of the compression strut formed in the loaded concrete member, the three-dimensional principal stress space is transformed into two-dimensional space by means of the relation between the hydrostatic stress and the deviatoric stress. The analysis of the stress state in the compression strut revealed that the deviatoric stress increases with larger load particularly in the concrete surrounding the lower part of the shear stud. Accordingly, bearing failure of concrete occurred locally within a limited region in the slab. The steep increase of the deviatoric stress accompanying the increase of the load resulted in the failure of concrete around the lower part of the shear stud, which in turn provoked the deformation and the development of bending moment of the shear stud. Finally, plastic hinge formed in the shear stud leading it to reach its limit state. The proposed finite element model can also be used to model the shear connection of the composite beam and, the proposed stress analysis method can be applied to analyze its composite action behavior.
**Keywords:-** composite beam, push-out test, FEM analysis, composite action, shear connection

## I. INTRODUCTION

Being the primary components of the steel-concrete composite beam, the steel beam and the concrete slab are generally composed by means of shear connectors welded to the upper flange of the beam to form a monolithic structure. The structural behavior of the composite beam like its load-deflection relation and load-slip relation can vary according to the extent of composite action developed by the shear connectors. The extent of this composite action depends mainly on the type of shear connection, the material constants, the degree of composite action and the strength of concrete, among others. The characteristics of horizontal shear behavior at the steel-concrete interface needed for the structural design and analysis of the composite beam are usually derived from standard push-out test conducted on push-out specimens. However, previous studies reported the existence of definite differences in the shear composite behavior between the push-out specimen and the actual composite beam [1]-[9]. Concretely, the comparison of the designed and experimental values in these studies indicated that the composite beam designed with partial interaction sometimes behaved in reality as a composite beam with complete interaction.
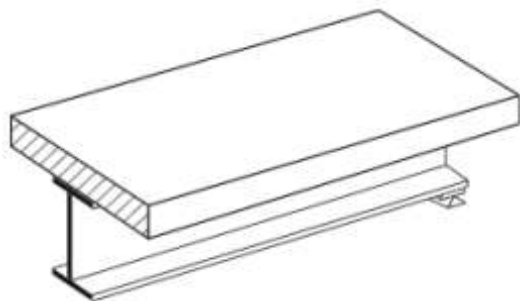


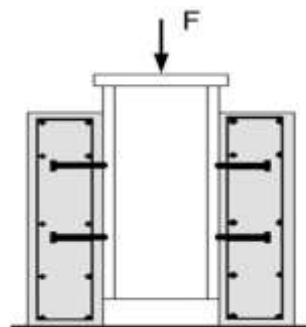**Fig. 1:** Steel-concrete composite beam          **Fig. 2:** Push-out specimen

This study intends to analyze the failure mechanism of the shear connection by three-dimensional finite element analysis (FEA) of push-out specimens that was practically unaffordable experimentally or numerically by two-dimensional FEA. The common push-out specimen is considered in the analysis for the verification of the structural performance of the shear connection. Based upon the suggested analytical method, another objective of this study is to propose a methodology enabling to investigate the difference between the results of

the analysis of the shear composite behavior of real composite beams and those of standard push-out test.

To that goal, the stress computed by three-dimensional FEA of the push-out specimen [4, 5] is exploited. Relevant formulae are then applied to obtain the three-dimensional principal stress contour and principal stress trajectory, which are used to examine the three-dimensional stress state of the concrete slab member. This stress state enables to investigate the local bearing failure of concrete known to be one major cause of the failure of the shear connection. The stress developed in concrete can generally be expressed by means of the triaxial stress state in the 3-dimensional principal stress space. In the present study, the 3-dimensional stress state is transformed into the hydrostatic stress and the deviatoric stress so as to ease effectively the analysis of the local failure of concrete around the shear connector in a 2-dimensional stress space. Moreover, the region over which the bearing failure of concrete may occur can be identified clearly and, its effect on the plastic behavior of the shear connector can be examined.

## II.     FEM MODEL OF PUSH-OUT SPECIMEN

The 3-dimensional FEA model shown in Fig. 3 was developed previously for the analysis of the structural behavior of push-out specimens[4, 5]. This model represents only the half of the specimen to improve the efficiency of the analysis. The material properties adopted in the analysis are 110 N/mm$^2$ for the compressive strength of concrete, 536 N/mm$^2$ for the tensile strength of the steel beam, and 550 N/mm$^2$ for the tensile strength of the shear stud [17]. The nonlinear stress-strain curve shown in Fig. 4 is applied in the concrete model. The triaxial compressive failure envelope in Fig. 5 and the triaxial tensile failure envelope in Fig. 6 are applied as failure criterion to assess the eventual tensile or compressive failure according to the stress state acting on the concrete element. Here, Fig. 5 showing the triaxial compressive failure envelope represents the expressions formulated in Equations (1) to (4). This triaxial compressive failure envelope adopted to the concrete model is proposed by Khan and Saugy[18] where $f_c$ and $f_{bc}$ is uniaxial and biaxial compressive strength, $\sigma_{oct}$ and $\tau_{oct}$ is hydrostatic and deviatoric stresses, $\sigma_{p1} \sim \sigma_{p3}$ are principal stresses, $I_1$ and $J_2$ is stress invariants. And tensile and tensile-compressive failure envelop is restricted by uniaxial tensile strength $f_{ct}$ and compressive strength $f_c$ shown in Fig. 6. Fig. 7 compares the analytical and experimental results [4, 5].
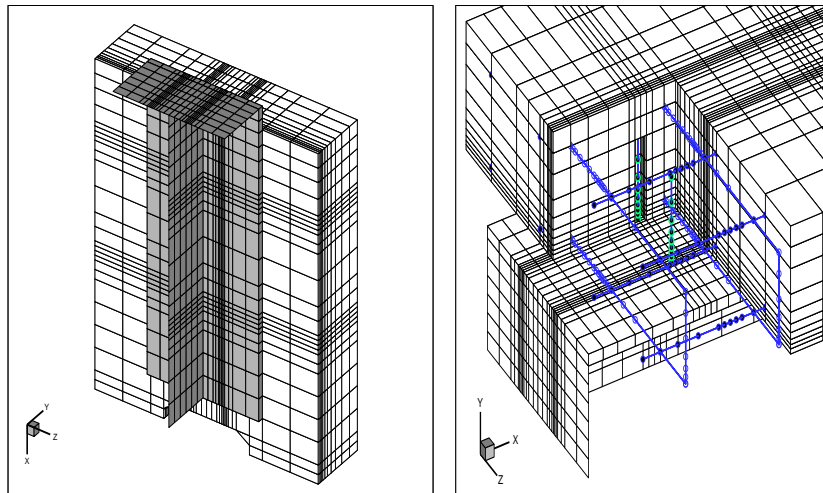


**Fig. 3:** FE model for the push-out test specimen [4, 5]

$$\alpha I_1 + \sqrt{J_2} - k = 0 \tag{1}$$

Where,

$$I_1 = \sigma_{p1} + \sigma_{p2} + \sigma_{p3} = 3\sigma_{oct} \tag{2}$$

$$J_2 = \frac{1}{6}\left[(\sigma_{p1} - \sigma_{p2})^2 + (\sigma_{p2} - \sigma_{p3})^2 + (\sigma_{p3} - \sigma_{p1})^2\right] = \frac{3}{2}\tau_{oct}^2 \tag{3}$$

$$\alpha = \frac{n-1}{\sqrt{3}(2n-1)}, \quad k = \frac{-n}{\sqrt{3}(2n-1)}, \quad n = \frac{\sigma_{bc}}{\sigma_c} \tag{4}$$
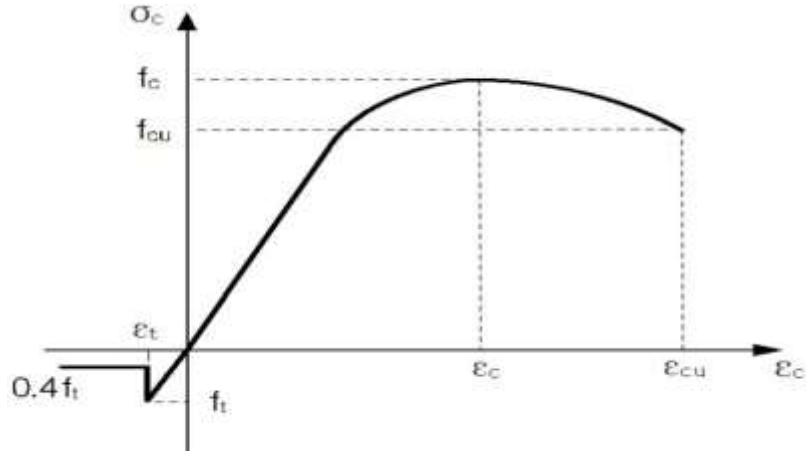
**Fig. 4:** Stress-strain curve of concrete [4, 5, 10, 11]
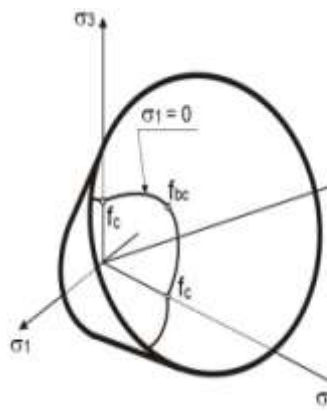


**Fig. 5:** Triaxial compressive failure
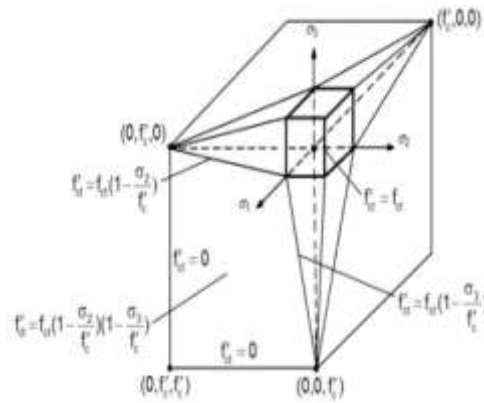envelope of concrete model [12]

**Fig. 6:** Triaxial tensile failure envelope
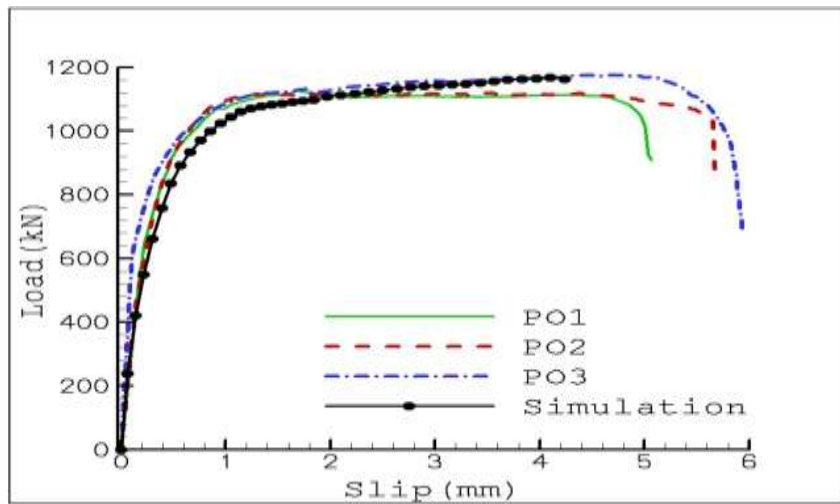of concrete model [13]



**Fig. 7:** Comparison of analysis and test results [4, 5]

## III. FAILURE MECHANISM OF SHEAR CONNECTION

The principal stress is computed by Equations (5) to (8) using the 3-dimensional stresses ($\sigma_1$, $\tau_{12}$, $\tau_{13}$, $\sigma_2$, $\tau_{21}$, $\tau_{23}$, $\sigma_3$, $\tau_{31}$, $\tau_{23}$) obtained from the FEA model presented in the previous chapter. In the equation (5) $\sigma_p$ is principal stress $\sigma_{p1}$, $\sigma_{p2}$ and $\sigma_{p3}$ which can be obtained by the equations. Fig. 8(a) shows the principal stress contour and the principal stress trajectory at the surface of the concrete member in contact with the flange of the steel beam. Here, the stress contour and trajectory are drawn for the largest absolute value of the principal stress

$\sigma_{p3}$ ($\sigma_{p1} > \sigma_{p2} > \sigma_{p3}$, negative for compressive stress) when reaching the limit state at which a shear force of about 137.5 kN acts upon the shear connector.

The external loading is transferred to the concrete member via the steel beam and the shear connectors. Fig. 8 shows the trajectory of the principal stress $\sigma_{p3}$ developed in the concrete member and propagating in a definite angle toward the bottom of slab from the point located beneath the interface between the shear stud and concrete. This trajectory agrees with the load path reported in previous studies and shown in Fig. 9. The difference in the contour and size of the stress observed at the bottom face at which the shear connector is welded to the steel flange and the top face of the concrete member can be explained as follows. Most of the load is transferred to the concrete member via the base of the shear connector but the force exerted locally on a limited region at the bottom concrete generates eccentric moment in the concrete member, which results in the occurrence of tensile stress at the top face of the concrete member and compressive stress at the bottom face.
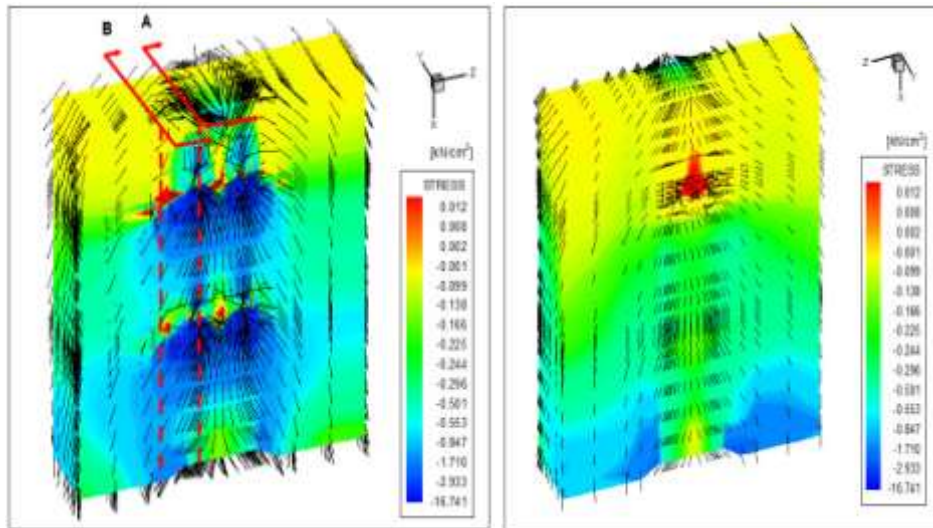
$$\sigma_p^3 + I_1\sigma_p^2 - I_2\sigma_p - I_3 = 0 \tag{5}$$

Where,

$$I_1 = \sigma_1 + \sigma_2 + \sigma_3 \tag{6}$$

$$I_2 = \sigma_1\sigma_2 + \sigma_2\sigma_3 + \sigma_3\sigma_1 - \tau_{12}^2 - \tau_{23}^2 - \tau_{31}^2 \tag{7}$$

$$I_3 = \sigma_1\sigma_2\sigma_3 + 2\tau_{12}\tau_{23}\tau_{31} - \sigma_1\tau_{23}^2 - \sigma_2\tau_{31}^2 - \sigma_3\tau_{12}^2 \tag{8}$$



|  (a) Bottom face  |  (b) Top face  |

**Fig. 8:** Principal stress contour and principal stress trajectory at the bottom and top face of concrete member
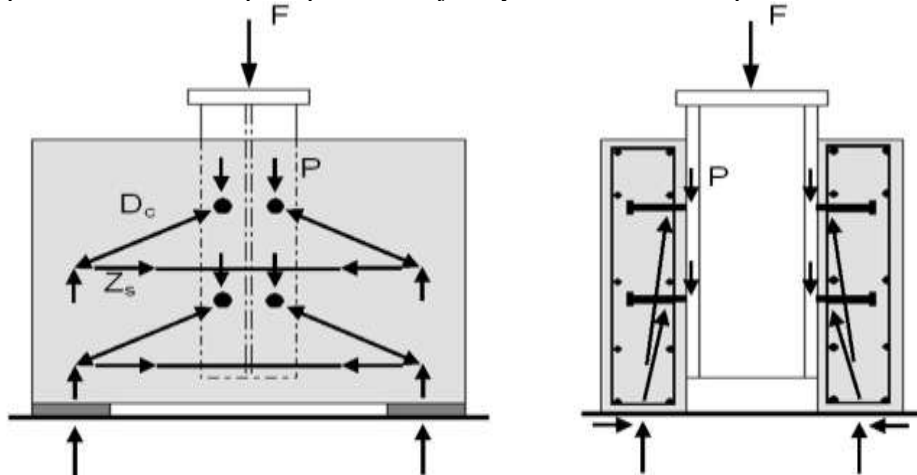


**Fig. 9:** Load transfer path in push-out specimen [14]

Fig. 10 draws the principal stress contour and the principal stress trajectory in sections A and B of the concrete member shown in Fig. 8(a). It appears that the stress concentrates in the concrete portion surrounding

the base of the shear connector and propagates with a definite angle. The comparison of the stress contour in these two sections reveals that the compressive stress developed in section A located closer to the shear connector is larger than that in section B.
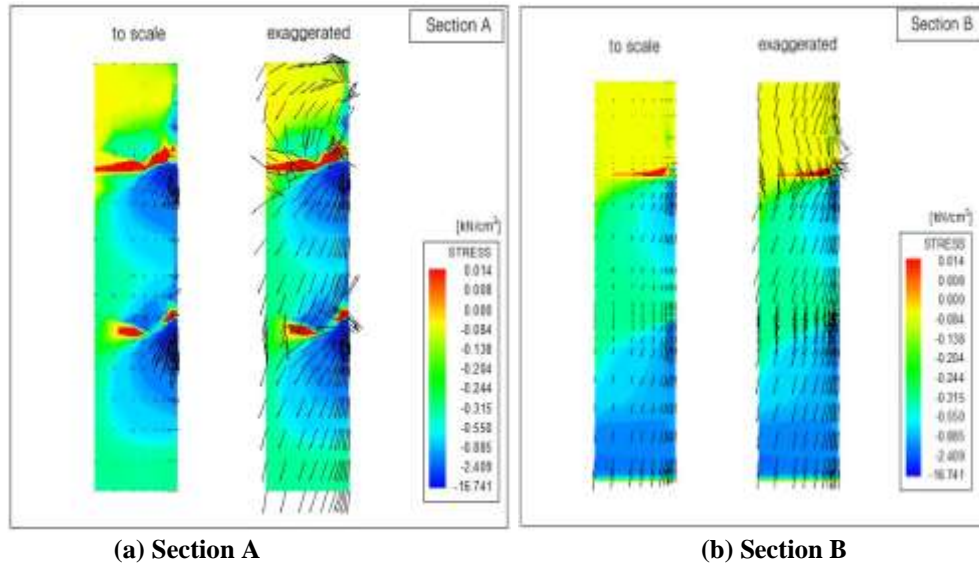


**(a) Section A**            **(b) Section B**
**Fig. 10:** Principal stress contour and principal stress trajectory in sections A and B of concrete member

If the load is applied at the center of the steel beam, this force is transferred to the concrete member via the shear studs. During this process, compression strut is formed within the concrete member (Fig. 11). The load transfer capacity of the shear connection, that is its load bearing capacity, depends on the type, cross-sectional area, and material strength of the shear stud but is also very closely related to the failure behavior of the concrete supporting the shear stud. Accordingly, if the 3-dimensional stress state of the compression strut formed in the concrete member can be analyzed, it would be possible to clarify further the failure behavior of the shear connection.
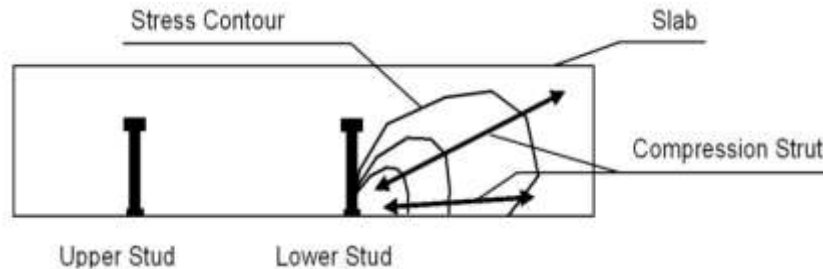


**Fig. 11:** Compression strut formed inside concrete member

The change in the state and size of the stress in the compression strut with respect to the external load can be analyzed using the graph proposed in Fig. 12 for example. In the graph, the lines passing through the uniaxial compressive strength ($f_c$) and the uniaxial tensile strength ($f_t$) can be expressed using Equation (9) and Equation (10), respectively. The stress state like compression (C)–compression (C), compression (C)–tension (T), tension (T)–compression (C) and tension (T)–tension (T) can be classified according to these two equations [15]. Moreover, the hydrostatic stress ($\sigma_{oct}$) and the deviatoric stress ($\tau_{oct}$) can be obtained using Equation (11) and Equation (12) [16]. The transformation of the 3-dimensional principal stress space into a stress space formulated by such relation between the hydrostatic stress and the deviatoric stress is done because the analysis is comparatively easier in the 2-dimensional space. In addition, the following reason can also be advanced in material engineering viewpoint. The triaxial stress state ($\sigma_{p1}, \sigma_{p2}, \sigma_{p3}$) can be considered as the sum of the two stress components of the hydrostatic stress ($\sigma_{oct}$) and deviatoric stress ($\tau_{oct}$). This means for example that the difference between the 3 principal stresses ($\sigma_{p1}, \sigma_{p2}, \sigma_{p3}$) becomes larger as much as $\tau_{oct}$ has higher value. When concrete is subjected to identical stresses in the three directions, the stress can be significantly higher than the uniaxial compressive strength ($f_c$). However, since the sizes of the 3 principal stresses differ to each other, the stress state becomes more unfavorable as much as the component contributed by $\tau_{oct}$ increases. Considering such material engineering principle, it appears that the eventual failure of concrete can be assessed by examining the

relative change of the deviatoric stress. In the equation (9) to (12) $\sigma_{p1}$, $\sigma_{p2}$ and $\sigma_{p3}$ are principal stresses, $\sigma_{oct}$ and $\tau_{oct}$ is hydrostatic and deviatoric stresses, and $I_1$ and $J_2$ is stress invariants.

$$\sqrt{J_2} + \frac{1}{\sqrt{3}}I_1 = 0 \tag{9}$$

$$\sqrt{J_2} - \frac{1}{\sqrt{3}}I_1 = 0 \tag{10}$$

$$\sigma_{oct} = \frac{1}{3}(\sigma_{p1} + \sigma_{p2} + \sigma_{p3}) \tag{11}$$

$$\tau_{oct} = \frac{1}{3}\sqrt{(\sigma_{p1} - \sigma_{p2})^2 + (\sigma_{p2} - \sigma_{p3})^2 + (\sigma_{p3} - \sigma_{p1})^2} \tag{12}$$
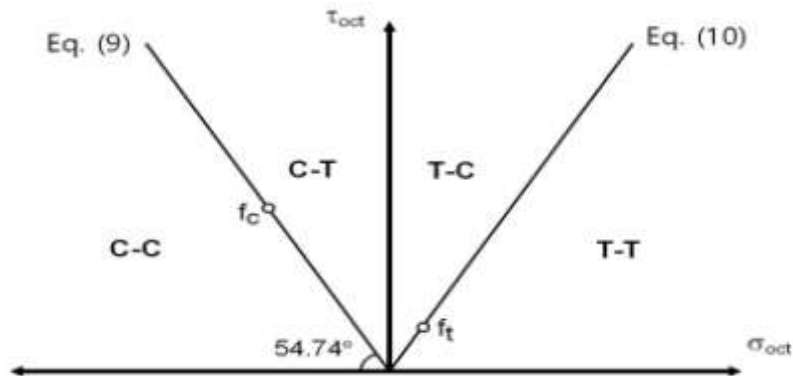


**Fig. 12:** Classification of concrete failure in hydrostatic-deviatoric stress space [15]

For instance, Fig. 13 shows graphically the hydrostatic-deviatoric stress relation for the compression strut formed in the concrete slab of the push-out specimen. In this example, the shear stud installed in the push-out specimen has diameter of 19 mm and tensile strength of 550 MPa, and the concrete member develops compressive strength of 110 MPa [17]. Fig. 13(a) presents the stress state obtained just before the start of the nonlinear behavior in the load-slip curve when a shear force of 62.3 kN applies on one shear stud. Fig. 13(b) depicts the stress state when the stud is near to its strength limit state under the application of a shear force of 137.5 kN. In the graphs, the values of the stress are indicated for concrete that can still transfer the load and the values for concrete that cannot transfer the compressive force anymore due to complete failure are discarded.

In view of the results, all the stress values in both cases fall around the limit between the compression (C)–compression (C) stress state and the compression (C)–tension (T) stress state. The stress exhibits generally larger values and the tensile cracks in the compression strut are seen to outnumber those under shear force of 62.3 kN when the shear force is 137.5 kN. This observation can be attributed to the fact that the deviatoric stress, which influences the failure of concrete, increases gradually with larger external load. As discussed above, when concrete is subjected to identical stresses in the three directions, it can support compressive stress higher than the uniaxial compressive strength but such ideal stress condition is rarely achieved in common structures. In the analysis example also, most values of the stress run outside the $\sigma_{oct}$ axis and fall around the limit between the compression (C)–compression (C) stress state and the compression (C)–tension (T) stress state, which is significant increase of the deviatoric stress. In other words, the deviatoric stress enlarges with the increase of the load and finally converges to the failure envelope to reach failure at the end.

Similarly, the analysis of the 3-dimensional stress state of the compression strut formed inside the concrete member shows that the increase of the deviatoric stress plays a determinant role in the failure of concrete. Based upon this concept, the region of concrete supporting the shear stud and undergoing failure can be easily identified by representing the profile of the deviatoric stress developed in the compression strut near the shear stud with respect to the height.

For example, the deviatoric stress exhibits various sizes over the horizontal section of the compression strut shown in Fig. 11. Fig. 14 plots the profile of the largest deviatoric stress along the height of the slab expressed as the distance from the base of the concrete member. Examining the state just before the occurrence of nonlinear behavior in the load-slip curve when a shear force of 62.3 kN applies on one shear stud, comparatively larger deviatoric stress is developed in the region running from the base to the height of about 2 cm. Besides, high deviatoric stress is seen to deploy up to the height of about 3.5 cm when the stud has nearly reached its strength limit state under application of a shear force of 137.5 kN. At the final stage, deviatoric stress up to $0.5f_c$ can be observed in this region.
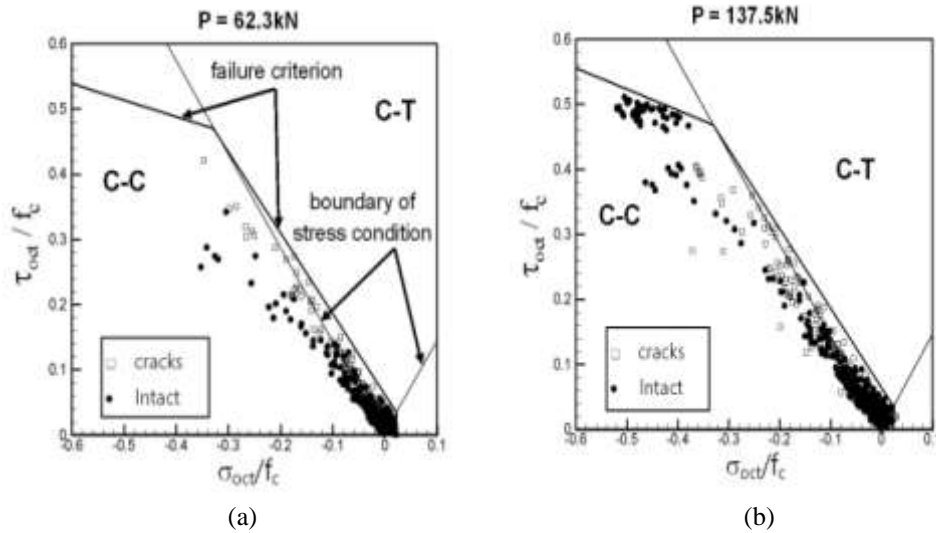
(a)                      (b)

**Fig. 13:** Change in stress state of compression strut according to loading stage
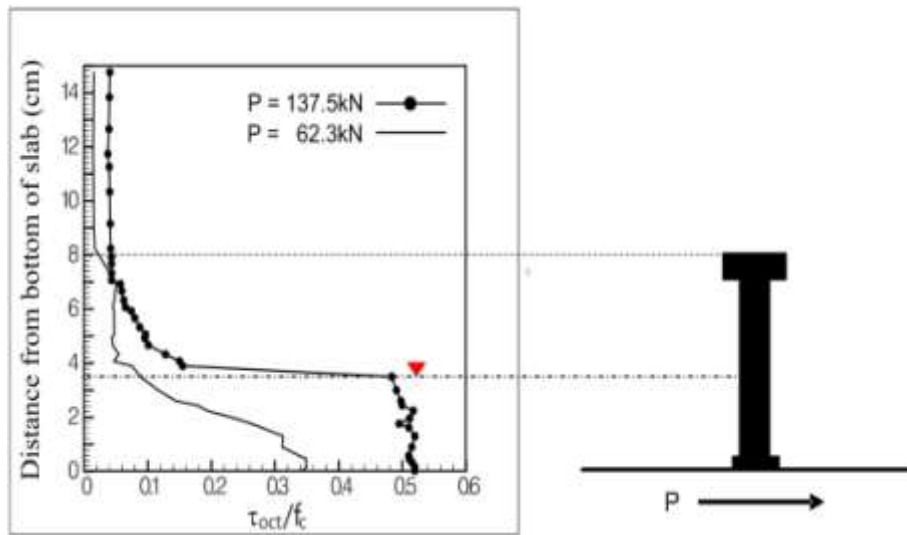


**Fig. 14:** Deviatoric stress profile according to slab height

Fig. 16 plots the bending moment developed in the shear stud section when the shear stud reaches the strength limit state. The plastic moment of the shear stud with diameter of 19 mm and yield strength of 540 MPa is 61.6 kN·cm. Referring also to the moment diagram in Fig. 16, it appears that plastic hinge has formed along a height of 0.5 to 2.5 cm from the bottom. The formation of the plastic hinge can be explained by the failure of concrete supporting the shear stud that led to the deformation and development of bending moment in the shear stud. In addition, the location of the plastic hinge is clearly closely related to the extent of failed concrete surrounding the stud because the length of the moment arm is determined by the extent of failed concrete. The extent of failed concrete would be smaller if concrete with higher strength is used or in case of a stress state in which the increase rate of the deviatoric stress remains minimal. In such case, the arm length of the moment acting on the stud will shorten and change the position of the plastic hinge, which consequently change the load bearing capacity of the shear connection. Further study should be conducted on this topic.

In view of the results, the failure behavior of the concrete surrounding the shear stud appears to play a critical role in the load bearing capacity of the shear connection. Moreover, such failure behavior of concrete is also very closely related not only to the material strength of concrete but also to the increase of the deviatoric stress occurring in the compression strut.
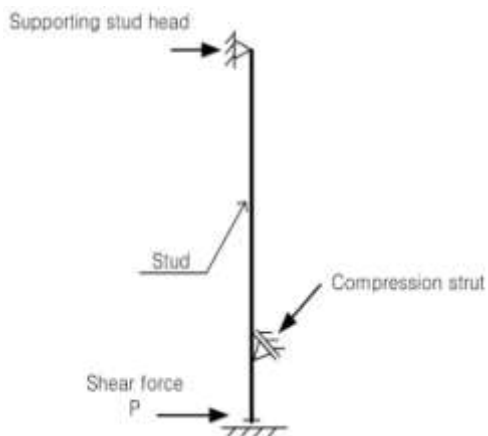
**Fig. 15:** Simplified analysis model of
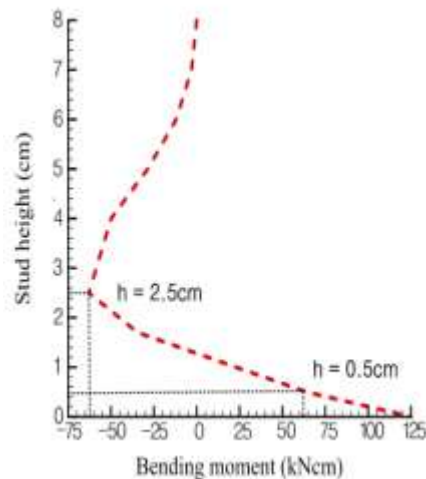stud in concrete slab

**Fig. 16:** Bending moment diagram
at strength limit state of stud

## IV. CONCLUSIONS

The load bearing capacity of the shear connection in push-out specimens is closely related to the failure behavior of the concrete surrounding the shear stud. The concrete surrounding the base of the shear stud undergoes gradual failure according to the increase of the external load that led to the deformation and development of bending moment in the shear stud, and the limit state is finally attained due to the formation of plastic hinge in the shear stud. Here, the failure behavior of concrete is very closely related not only to the material strength of concrete but also to the increase of the deviatoric stress occurring in the compression strut. This study analyzed the stress state by transforming the 3-dimensional principal stress space into a 2-dimensional stress space representing the relation between the hydrostatic stress and the deviatoric stress. This transformation made it possible to examine quantitatively the failure behavior of the compression strut formed in the concrete member of the push-out specimen and to identify the failure mechanism of the shear connection. The proposed finite element model can also be used to model the shear connection of the composite beam and, the proposed stress analysis method can be applied to analyze its composite behavior.

### REFERENCES

[1]. H. Bode, J. Schanzenbach, "Das Tragverhalten von Verbundträgern bei Berücksichtigung der Dübel-nachgiebigkeit", Stahlbau 58, Heft 3, pp. 65-74, 1989.

[2]. H. Bode, European Steel-Concrete Composite Structure, Construction and Calculation, Werner Verlag, 1998.

[3]. R. P. Johnson, Composite Structures of Steel and Concrete, volume 1: Beams, Columns, Frames and Applications in Building, London, 1975.

[4]. H. S. Shin, A Contribution to the Numerical Analysis of the Load Carrying Behaviour of the Composite Beams with High Strength Steel and High Strength Concrete, Dissertation, RWTH-Aachen University, 2004.

[5]. H. S. Shin, FEM Analysis of the Horizontal Shear Behaviour in the Steel-Concrete Composite Beam, International Journal of Engineering Research and Development, Volume 10, Issue 9, 2014.

[6]. A. Shariati, N. H. RamliSulong, MeldiSuhatril, M. Shariati, "Various Types of Shear Connectors in Composite Structures": A Review, International Journal of Physical Sciences, Vol.7, no.22, pp.2876-2890, 2012.

[7]. M. G. Navarro, J. P. Lebet, "Tests on Cracked Composite Beams for Bridges", Theori und Praxis im konstruktiven Ingenieurbau, Festschrift zu Ehren von Prof. Dr.-Ing. H. Bode, Ibidem Verlag, pp.521-532, Stuttgart, 2000.

[8]. J. M. Aribert, "Application and Recent Development of a Numerical Model for Composite Beams with Partial Shear Connection", Composite Construction in Steel and Concrete II, Proceedings of an Enginnering Foundation Conference, pp.742-757, Potosi, Missouri, USA, 1992.

[9]. J. M. Aribert, A. Al Bitar, Optimization of the Design in Partial Connection of Beams in Composite Floors with Thin Profiled Steel Sheeting, Construction Metallique, No.4, pp.3-33, 1989

[10].  A. Sokolov, G. Kaklauskas, S. Idnurm, V. Gribniak, D. Bacinskas, "Tension-Stiffening Model Based on Test Data of RC Beams", The 10th International Conference of Modern Building Materials, Structures and Techniques, pp.810-814, 2010.

[11].  G. König, E. Fehling, "Zur Riss Breitenbeschränkung im Stahlbetonbau", Beton- und Stahlbetonbau 83, Heft 6, pp.161-167, 1988.

[12].  M. H. Khan, B. Saugy, "Evaluation of the Influence of Some Concrete Characteristics on Nonlinear Behaviour of Prestressed Concrete Reactor Vessel", ACI Publication SP-34, pp.159-179, 1972.

[13].  K. J. Bathe, S. Ramaswamy, "On Three-Dimensional Nonlinear Analysis of Concrete Structures", Nuclear Engineering and Design 52, pp.385-409, 1979.

[14].  Roik, K., Bergmann, R., Haensel, J., Hanswille, G., Verbundkonstruktionen, Bemessung auf der Grundlage des Eurocode 4 Teil 1. In: Betonkalender 1993, Ernst & Sohn Verlag, Berlin, p.551, 1993.

[15].  Stempniewski, L., Eibl, J.: Finite Elemente im Stahlbeton. Beton Kalender, Teil 1, Ernst & Sohn Verlag, 1993

[16].  Boresi, A.P., Sidebottom, O.M., Seely, F.B., Smith, J.O., Advanced Mechanics of Materials, John Willy and Sons, 1978.

[17].  Hoffmeister, B., Sedlacek, G., Müller, Ch., Use of High Strength Steel S460, Composite beams made of high strength steel and high strength concrete, RWTH Aachen, 2000.

[18].  M. H. Khan, B. Saugy, "Evaluation of the Influence of Some Concrete Characteristics on Nonlinear Behaviour of Prestressed Concrete Reactor Vessel", ACI Publication SP-34, pp.159-179, 1972.